Applied Catalysis B: Environmental 165 (2015) 296–305

Contents lists available at ScienceDirect

Applied Catalysis B: Environmental

journal homepage: www.elsevier.com/locate/apcatb

K-promoted NiMo catalysts supported on activated carbon for the hydrogenation reaction of CO to higher alcohols: Effect of support and active metal

E.T. Liakakou[a,b], E. Heracleous[a,c,*], K.S. Triantafyllidis[a,d], A.A. Lemonidou[a,b]

[a] Chemical Process & Energy Resources Institute (CPERI), Centre for Research and Technology Hellas (CERTH), 6th km Charilaou – Thermi Road, P.O. Box 361, 57001 Thessaloniki, Greece
[b] Department of Chemical Engineering, Aristotle University of Thessaloniki, P.O. Box 1517, 54124 Thessaloniki, Greece
[c] School of Science & Technology, International Hellenic University (IHU), 14th km Thessaloniki – Moudania, 57001 Thessaloniki, Greece
[d] Department of Chemistry, Aristotle University of Thessaloniki, P.O. Box 116, 54124 Thessaloniki, Greece

ARTICLE INFO

Article history:
Received 1 August 2014
Received in revised form 3 October 2014
Accepted 10 October 2014
Available online 22 October 2014

Keywords:
CO hydrogenation
Higher alcohols
K-promoted Ni—Mo catalysts
Activated carbon
Acidity

ABSTRACT

This study investigates the effect of active metal and the nature and pre-treatment of the support in a series of K-promoted NiMo catalysts supported on activated carbon (AC) for the hydrogenation reaction of CO. The Ni—Mo synergistic effect was found to be essential for the activation of CO. The use of activated carbon as support led to a three-fold increase in the selectivity toward higher alcohols, compared to the unsupported material, probably due to a reduction in the crystallinity of the active $NiMoO_4$ phase and its partial transformation from alpha to beta form. Pre-treatment of the activated carbon prior to its use as support with HNO_3 aqueous solution led to significant increase in CO conversion, related to the lower amount of ash and the much higher acidity of the acid treated sample. The use of a higher surface area acid-treated support also increases activity, with the K—NiMo/AC2a catalyst exhibiting a 45% higher conversion at 280 °C compared to K—NiMo/AC1a. The improvement in activity can be ascribed to better dispersion of the active phase on the higher surface area AC support and therefore higher exposure of active Ni—O—Mo sites. Overall, the K—NiMo/AC2a catalyst exhibited the optimum performance, with high CO conversion (25% at 280 °C) and high production of oxygenates, with a space time yield to oxygenates of 141.5 mg/$g_{catalyst}$/h at 280 °C. A clear tendency of increasing higher alcohol production with decreasing acidity was evidenced for all K-promoted bimetallic NiMo catalysts.

1. Introduction

Gasification of biomass to syngas and its subsequent conversion to hydrocarbons via the Fischer–Tropsch reaction has been identified as a promising process for the production of "green", high quality transportation fuels. Moreover, this process is one of the few alternative processes that can produce sustainable fuels for the aviation sector, where the specifications are extremely stringent. In the frame of the EU-funded project EuroBioRef, several bio-based components derived from lignocellulosic biomass were developed and evaluated as aviation fuels. Besides hydrocarbons, higher alcohols were also identified as highly promising and suitable components for jet fuel [1]. These higher alcohols can be produced thermochemically in a process similar to BtL-Fischer–Tropsch, with a different catalyst in the F-T synthesis reaction in order to drive CO hydrogenation to higher alcohols formation rather than hydrocarbons.

Typical catalysts investigated for the hydrogenation of CO to higher alcohols and oxygenates include modified low and high temperature Cu-based methanol synthesis catalysts, modified Co and Fe Fischer–Tropsch catalysts and Mo-based materials in oxidic and sulfided form [2–4]. Higher alcohol synthesis (HAS) on Mo and Group VIII metals has been extensively studied since the 1980s [2–6]. A great advantage of Mo-based catalysts is their excellent resistance to sulfur poisoning. The addition of alkali metals was found to shift selectivity for CO hydrogenation from hydrocarbons to alcohols [7]. Li et al. [8] reported that K doping on AC-supported pre-reduced (non-sulfided) molybdenum catalysts significantly promotes the formation of alcohols at the expense

* Corresponding author at: Chemical Process & Energy Resources Institute (CPERI), Centre for Research and Technology Hellas (CERTH), 6th km Charilaou – Thermi Road, P.O. Box 361, 57001 Thessaloniki, Greece. Tel.: +30 2310 498345; fax: +30 2310 498380.
E-mail address: eheracle@cperi.certh.gr (E. Heracleous).

http://dx.doi.org/10.1016/j.apcatb.2014.10.027
0926-3373/

of CO conversion to hydrocarbons. In a recent work by Surisetty et al. on MoS_2 catalysts [9], it was suggested that activity is also influenced as the increase of K loading was found to increase Mo dispersion and the number of active sites in MoS_2 domains. In addition, alkali promotion seems to be essential for achieving high catalyst stability [10]. Muramatsu et al. [11] claimed that the role of K on pre-reduced Mo/SiO_2 is to preserve some surface MoO_2 species which are active for alcohol synthesis.

Selectivity to alcohols on alkali promoted Mo catalysts normally follows the Anderson-Schultz-Flory distribution, which limits higher alcohol formation. However, further promotion with transition metals like Co and Ni was shown to improve C_{2+} alcohol selectivity [12–15]. When K/MoS_2 was co-modified with Ni and Mn, the synergistic effect of both promoters enhanced the catalytic activity and the formation of C_2–C_3 alcohols [12]. It was suggested that Ni enhances the $C_1 \rightarrow C_2$ homologation step, which might explain the high ethanol selectivity [6].

Supporting the Mo active phase on a high surface area refractory material can be beneficial as it increases the number of active sites via enhanced dispersion and distribution of the metal particles over the support. According to a review by Surisetty et al. [6], typical supports, such as various types of carbon, alumina, silica, and zirconia, have been tested in higher alcohols synthesis catalysts. The support effect was found to depend strongly on the state of the active phase (metal, oxide, sulfide). Bartholomew et al. [16] reported that the support greatly influences initial and steady state activities of reduced Mo catalysts, while the activities of sulfided Mo catalysts are, with the exception of MoS_2/C, independent of support. Acidic supports, such as Al_2O_3 and ZrO_2, were found to suppress the formation of alcohols and increase the hydrocarbon formation reaction rate on pre-reduced Mo catalysts, rendering neutral or basic supports more suitable. Activated carbon is a neutral catalyst support, with large surface area, limited interaction between support and active phase, resistance to acidic or basic media, and stability at high temperatures and pressures [6]. The beneficial effect of carbon supports (activated carbon and carbon nanotubes) on pre-reduced and sulfided Mo catalysts has been reported in literature by several groups [16–19]. Ma et al. [18] studied the effect of acid treated AC support on a pre-reduced $K_{0.5}$—Ni_1—Mo_1 catalyst for the CO hydrogenation reaction. The use of the AC support was found to greatly increase selectivity to oxygenates (>40%, CO_2 free basis at 50 bar and 265 °C) compared to the unsupported reference catalyst, although significant amounts of dimethylether were also formed. Doping of sulfided $Ni_{0.5}Mo_1K_{0.5}$ with multi-walled carbon-nanotubes also resulted in 12% increase of the oxygenated products space time yield, with a minor decrease in total oxygenates selectivity [19]. It has been postulated that the interaction of carbon with the Ni—Mo components prevents the complete reduction of the active metals (which leads to methane formation) and preserves partially oxidized Mo and Ni sites which are active for alcohol formation [18].

In this study, we investigate the hydrogenation of CO to higher alcohols over K-promoted monometallic and bimetallic nickel-molybdenum oxide-based catalysts supported on activated carbon (AC), focusing on the effect of acidity. Although acidity has been identified as a crucial factor for the activity and product distribution in CO hydrogenation [6,16,20 and references therein], literature studies on Mo-based catalysts have not explicitly addressed the effect of acidity and its relation to the catalytic performance in CO hydrogenation. The influence of the type of the carbon used as support was examined by employing two activated carbons with significant differences in surface area. The effect of pre-treating the activated carbon with acid to remove ash prior to impregnation and form surface carbon–oxygen complexes that can enhance metal dispersion on the support [21] was also investigated. Physicochemical characterization results are combined with catalyst evaluation data in higher alcohol synthesis in an attempt to identify the different functionalities of the AC support and the nature of active sites.

2. Experimental part

2.1. Catalyst preparation

Two commercial activated carbons, Norit D10 and Norit SAE Super, with surface areas of 600 and 1200 m^2/g respectively, were used as supports; they were denoted as AC1 and AC2, respectively. The supports were used either as supplied or after acid treatment with a 50 vol% HNO_3 aq. solution at room temperature overnight, followed by thorough washing with de-ionized water and drying at 110 °C for 8 h (referred to as ACXa and ACXb for the acid-treated and untreated supports respectively). The supports were then impregnated with the active metals with the procedure described below. For characterization reasons and in order to simulate the state of the supports in the final catalysts, a quantity of the supports either as supplied or after acid treatment was calcined at 575 °C for 4 h under N_2 atmosphere. These materials are denoted as $ACX(a\ or\ b)_{calc}$.

The supported K-promoted monometallic and bimetallic catalysts were prepared by a stepwise incipient wetness method, with a constant K/Ni/Mo molar ratio of 0.05/1/1. The loading of the active phase was kept constant at 35 wt% for the bimetallic catalysts, while the loading of Ni and Mo in the monometallic samples was equal to 13.4 wt% and 21.6 wt% respectively (equal to the corresponding content of each metal in the bimetallic samples). For the monometallic samples, an aqueous solution containing the appropriate stoichiometric amount of either $(NH_4)_6Mo_7O_{24}{\cdot}4H_2O$ (Aldrich) or $Ni(NO_3)_2{\cdot}6H_2O$ (Aldrich) was impregnated via incipient wetness in a stepwise manner in the activated carbon support, followed by drying at 110 °C for 10 h. In the case of the bimetallic catalysts, the support was first impregnated with Mo and after drying at 110 °C for 6 h, the appropriate amount of nickel was sequentially impregnated in the above Mo loaded catalyst. In all cases, the materials were then dried at 110 °C for 10 h and calcined at 575 °C for 4 h under N_2 atmosphere. The potassium promoter was added on the resulting solids by dry impregnation with an aqueous solution of K_2CO_3 (Aldrich), followed by drying at 110 °C for 6 h and final calcination at 400 °C for 4 h under N_2.

Additionally, an unsupported reference NiMoK mixed oxide with a constant K/Ni/Mo molar ratio of 0.05/1/1 was prepared by the evaporation method. An aqueous solution containing the precursor salts, $(NH_4)_6Mo_7O_{24}{\cdot}4H_2O$ (Aldrich) and $Ni(NO_3)_2{\cdot}6H_2O$ (Aldrich), in appropriate amounts was heated at 70 °C under continuous stirring for 1 h to ensure complete dissolution and good mixing of the starting compounds. The solvent was then removed by evaporation under reduced pressure and the resulting solid was dried overnight at 110 °C and calcined at 575 °C for 4 h under N_2 atmosphere. The potassium promoter was then added using the exact procedure as that described above.

2.2. Catalyst characterization

Inductive coupled plasma-atomic emission spectroscopy (ICP-AES) was used for the determination of the chemical composition of the materials, using a Plasma 400 (Perkin Elmer) spectrometer, equipped with Cetac6000AT+ ultrasonic nebulizer.

For the determination of surface area (BET method) and pore volume, N_2 adsorption/desorption experiments were conducted at −196 °C, using an Automatic Volumetric Sorption Analyzer (Autosorb-1MP, Quantachrome). The total pore volume was determined at $P/P_0 = 0.99$ and the micropore volume was deduced from

t-plot analysis (de Boer method). Prior to the measurements, the samples were dehydrated in vacuum at 250 °C overnight.

X-ray diffraction (XRD) measurements were performed using a SIEMENS D-500 diffractometer employing CuKα_1 radiation (λ = 0.15405 nm) and operating at 40 kV and 30 mA. The XRD patterns were accumulated in the range of 5–75° 2θ every 0.02° (2θ) with counting time 2 s per step.

The reduction characteristics of the catalysts were studied by temperature programmed reduction (TPR) in a home-made gas flow system equipped with a fixed bed flow reactor and a quadrupole mass analyzer (Omnistar, Balzers). Typically, the catalyst sample (200 mg) was placed in the quartz reactor and was pretreated in flowing He for 0.5 h at 350 °C, followed by cooling at room temperature. The temperature was then raised from room temperature to 800 °C with a heating rate of 10 °C/min in a 5%H_2/He flow (50 cm^3/min). The main (*m*/*z*) fragments registered were: H_2 = 2, H_2O = 18, CO = 28 and He = 4.

NH_3-temperature programmed desorption (TPD-NH_3) was used to determine the acid properties. Experiments were performed on the same apparatus as described above. The catalysts (200 mg) were pretreated at 350 °C for 0.5 h and then cooled to 100 °C under He flow. The pretreated samples were saturated with 5% NH_3/He for 1 h at 100 °C, with subsequent flushing with helium at 100 °C for 3 h to remove the physisorbed ammonia. TPD analysis was carried out from 100 °C to 700 °C, at a heating rate of 10 °C/min. The (*m*/*z*) fragments registered were as follows: NH_3 = 15; H_2O = 18; N_2 = 28; NO = 30; N_2O = 44 and NO_2 = 46. Quantitative analysis of the desorbed ammonia was based on (*m*/*z*) 15.

2.3. Catalytic reaction tests

The catalytic performance of the samples in carbon monoxide hydrogenation was evaluated in a high pressure small-scale test unit, equipped with three gas lines controlled by high accuracy mass flow controllers. The unit operates with a stainless steel fixed bed reactor (ID: 9.3 mm), externally heated with a three-zone furnace, while the exit stream of the reactor is cooled via a heat exchanger and is directed to a system of vessels for the separation and collection of the liquid and gaseous products. The reaction temperature is monitored with a thermocouple inserted in the catalytic bed. The test facility can operate to a temperature range up to 600 °C and pressures up to 100 atm.

The samples were first diluted with equal amount of SiC particles of the same size to achieve isothermal operation and were then loaded in the fixed bed reactor, where they were treated in situ under pure hydrogen at 350 °C for 12 h and atmospheric pressure. These pre-treatment conditions were chosen to stabilize the catalyst surface under reductive atmosphere at higher temperature than reaction conditions [16,18]. The higher alcohol synthesis reaction was investigated in the temperature range 250–280 °C at 60 bar, *W*/*F* ratio of 0.63 g s/cm^3 and inlet feed composition H_2/CO = 2. The steady-state activity measurements were taken after at least 24 h on-stream. The gaseous products were analyzed on-line, while liquids were collected in a trap (−15 °C) for 24 h and were analyzed offline. The analysis was performed with a GC Agilent 7890A equipped with two detectors (FID & TCD) and three columns (MS, Porapak Q and DB-FFAP) in a series-bypass configuration.

CO conversion was calculated as the mole percentage of carbon monoxide converted to products:

$$\text{CO conversion (mol\%)} = \frac{\text{moles of CO}_{in} - \text{moles of CO}_{out}}{\text{moles of CO}_{in}} \times 100 \quad (1)$$

Carbon selectivity was defined as the moles of carbon in a given product to the total moles of converted carbon:

$$\text{Selectivity(C mol\%)} = \frac{\text{moles of a given product} \times \text{number of carbons in product}}{\text{moles of CO}_{in} - \text{moles of CO}_{out}} \quad (2)$$

Space time yield (STY) was calculated as the weight of each oxygenated compound produced per unit mass catalyst and per time unit:

$$\text{STY (mg/g}_{cat}\text{ h)} = \frac{\text{weight of oxygenated compound}}{\text{catalyst weight} \times \text{time}} \quad (3)$$

3. Results

3.1. Catalyst characterization

3.1.1. Characterization of the activated carbon supports

The main physicochemical characteristics of the two activated carbons as-received, after acid treatment and after calcination are provided in Table 1. The BET measurements show that both the commercial activated carbons have high surface areas, with AC2 demonstrating almost double surface area and pore volume than AC1. The N_2 adsorption isotherms of both carbons (Figure S1 in Supplementary) belong to a mixed type in the IUPAC classification [22]: type I due to the microporous nature of ACs and type II attributed to multilayer N_2 sorption that could occur on the plate-like carbon particles. A clear hysteresis loop of H4 type correlated with the slit-like pores generated within the plate-like particles can also be seen. Based on the type of the isotherms and the data in Table 1, it can be suggested that both activated carbons are mainly microporous materials with similar micropore surface and volume, while AC2 exhibits a much larger portion of meso/macroporosity and external area compared to AC1. The presence of mesopores together with micropores in activated carbons has been also shown in previous studies [23].

Acid treatment of the activated carbons was performed in order to remove the inorganic constituents (ash) in the supports and also form surface carbon–oxygen complexes that can enhance the metal dispersion on the AC support, as has been also suggested by other researchers [18,21]. Treatment of the supports with 50% aqueous HNO_3 solution does not lead to significant changes of surface area and pore volume of either activated carbon sample (Table 1), indicating that the texture and morphology of the carbons are not

Table 1
Physicochemical characteristics of the activated carbon supports.

Samples	Surface area (m^2/g)		Pore volume (cm^3/g)		Acidity (10^{-8} mol NH_3/m^2)
	Microporous	Total	Microporous	Total	
AC1	351	600	0.14	0.41	3.3
AC1a	380	570	0.15	0.36	7.6
$AC1a_{calc}$	400	580	0.17	0.39	4.7
AC2	392	1150	0.17	0.85	1.1
AC2a	319	1159	0.13	0.85	4.2
$AC2a_{calc}$	331	1184	0.14	0.87	1.6
$AC2b_{calc}$	316	1145	0.13	0.85	1.2

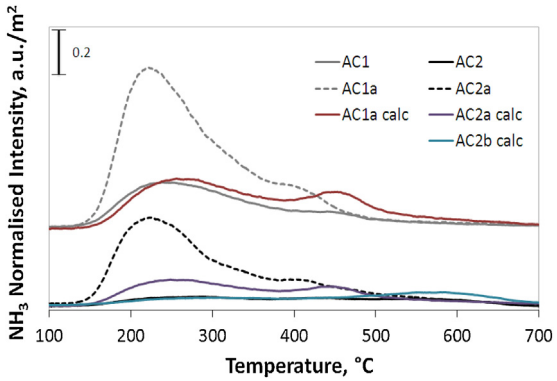

Fig. 1. Ammonia desorption profiles of the activated carbon supports.

significantly altered in this relatively mild acidic media. The ash content of the activated carbons prior and after acid treatment was determined by TGA analysis under air flow up to 800 °C (see Supplementary material, Figure S2. The high surface area activated carbon AC2 was found to have a much higher ash content than AC1 in the untreated form (15.2 wt% compared to 5.5 wt%). The acid treatment induced a 60% and 27% ash removal from AC1 and AC2 respectively. These results were confirmed by ICP chemical analysis, based on determination of the most abundant metals contained in inorganic ash (Table S1 in Supplementary material). The ICP measurements agree qualitatively with the TGA results and clearly show that ash is drastically reduced after acid treatment on both samples.

Ammonia-TPD was performed for determining the influence of acid treatment on the surface acidity of carbons. The ammonia desorption curves of the AC supports before, after acid treatment and after calcination, are compiled in Fig. 1 and the acidity results (expressed as mol of desorbed NH_3/m^2) are shown in Table 1. The TPD-NH_3 profiles of all carbon samples exhibit desorption peaks in two different temperature ranges: 150–300 °C and 400–500 °C. These peaks can be tentatively assigned to acid sites of weak and medium/high strength, respectively. The treatment with HNO_3 causes a large increase in the concentration of weak acid sites for both carbons, which can be attributed to the formation of acidic functional groups (such as —COOH and —OH) on their surface. The increased weak acidity could also be due to the removal of inorganic compounds by the acid, leaving sites on the carbon surface which can chemisorb oxygen in air at room temperature. This would result in more oxygen surface complexes which can generate acidic sites [21]. After calcination at 575 °C, the number of acid sites is reduced significantly indicating that the formed functional groups largely decompose at this temperature. However, the acidity of the calcined acid-treated samples is higher than that of the original supports, both for AC1 and AC2. On the contrary, the calcined untreated AC2b sample demonstrates the same acidity value as the mother support. This confirms that acid treatment leads to creation of thermally stable acidic functionalities on the surface of the activated carbons.

3.1.2. Characterization of the K-promoted mono- and bi-metallic NiMo catalysts

The main physicochemical characteristics of all K-promoted mono- and bi-metallic NiMo catalysts investigated in the present work are shown in Table 2. ICP analysis shows that the intended chemical composition is largely achieved in all the calcined catalysts. Concerning the textural properties, the unsupported K—NiMo oxide was found to have a very low surface area (25 m^2/g). The effect of impregnating the various metals on the porous characteristics of the lower surface area carbon (AC1) is pronounced in the case of the monometallic K—Mo/AC1a and bimetallic K—NiMo/AC1a

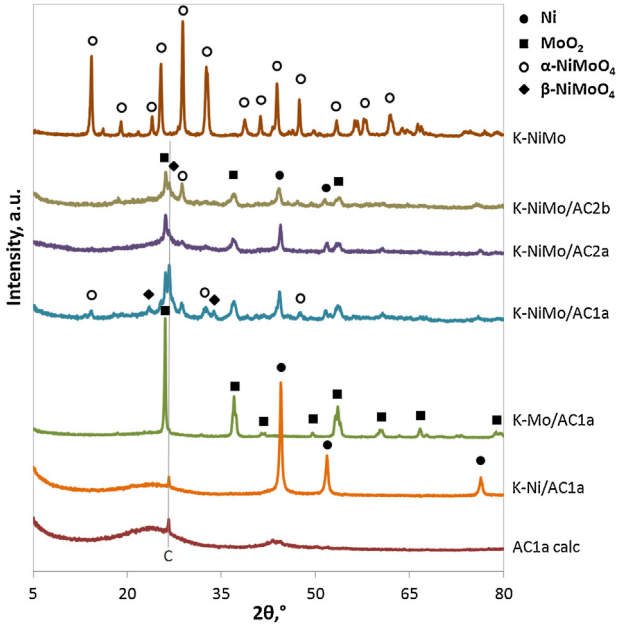

Fig. 2. X-ray diffraction patterns of the K-promoted mono- and bi-metallic NiMo catalysts and reference unsupported K—NiMo and $AC1a_{calc}$ support.

catalysts, where ~50% reduction is recorded compared to the parent support. The decrease is similar in both micropore and mesopore surface area and volume. The effect is less severe when these values are normalized on the basis of the carbon weight of the catalysts, since the loaded metals/oxides constitute about 30–50% of the catalyst mass. On the contrary, no reduction is measured for the monometallic nickel-based catalyst. The nickel-based catalyst consists only of a metallic nickel phase, whereas the Mo-containing samples contain oxidic MoO_2 and $NiMoO_4$ phases (see XRD results below). It could be postulated that the presence of Mo-oxides causes a notable blockage of the pores of the activated carbon support, whereas the metallic Ni particles (which are expected to have a smaller particle size) leave the surface unaffected.

A similar decrease of micropore surface area and pore volume is observed for the AC2 supported catalysts; however, a pronounced decrease of the meso/macropore area and pore volume as high as 70% occurs for these catalysts. This reduction can be attributed to meso/macropore blockage of the high surface area activated carbon AC2 due to the high active metal loading [21,24]. Concerning the effect of acid treatment, a slightly higher decrease in surface area and pore volume is recorded for the acid treated carbon based catalyst K—NiMo/AC2a compared to the untreated K—NiMo/AC2b. It can be postulated that metal ions can defuse easier into both the micro- and mesopores of the acid treated carbon causing a higher pore blockage [21].

X-ray Diffraction (XRD) was employed in order to identify the crystalline phases in the investigated catalysts. Fig. 2 illustrates the diffractograms obtained for all catalytic samples. The XRD pattern of the calcined acid treated AC1 support reveals a largely amorphous material. The two wide diffractions at 22° and 43° can be assigned to the sample holder used, while the small sharp peak at 26.6° to crystalline graphitic carbon [25]. Similar diffractograms were recorded for all other activated carbon supports examined in the present study and are not presented for brevity. The only diffraction peaks detected for K—Ni/AC1a, apart from the carbon phase of the support, can be clearly assigned to metallic Ni. According to Wang and Lu [21], the nickel nitrate precursor deposited on carbon decomposes to NiO at 200–300 °C, which is further reduced to metallic Ni at ~500 °C under an inert nitrogen atmosphere. No

Table 2
Physicochemical characteristics of the calcined K-promoted mono- and bi-metallic NiMo catalysts.

Samples	Nominal composition (wt%)			ICP composition (wt%)			Surface area (m^2/g)		Pore volume (cm^3/g)		H_2 consumption (mmol/g)	CO production (mmol/g)	Acidity (10^{-8} mol NH_3/m^2)
	Ni	Mo	K	Ni	Mo	K	Micro	Total	Micro	Total			
K—Ni/AC1a	13.4	–	0.4	19.7	–	0.2	420	606	0.17	0.37	4.2	1.2	2.6
K—Mo/AC1a	–	21.6	0.4	–	20.5	0.3	207	304	0.08	0.20	3.3	3.6	8.0
K—NiMo/AC1a	13.4	21.6	0.4	15.1	19.8	0.3	218	325	0.09	0.25	5.9	3.2	27.5
K—NiMo/AC2a	13.4	21.6	0.4	13.3	21.6	0.4	177	425	0.08	0.29	4.9	3.1	35.2
K—NiMo/AC2b	13.4	21.6	0.4	15.3	24.1	0.3	217	475	0.09	0.33	4.1	3.3	26.9
K—NiMo	26.6	43.5	0.9	33.0	50.0	0.8	3	25	0.001	0.15	7.3	0.2	57.5

K-containing crystalline phases were identified, indicating that the alkali promoter is amorphous and/or finely dispersed on the surface in nanoparticles. For K—Mo/AC1a, MoO_2 is the only crystal phase formed. In the case of molybdenum which is less reducible than nickel, it seems that the decomposition of the precursor that takes place up to 575 °C in N_2 leads to partial reduction of the formed Mo species from Mo(VI) to Mo(IV), with the activated carbon acting as reducing agent, as reported by Li et al. [26].

Concerning the K-promoted bimetallic catalysts, it can be observed that the unsupported K—NiMo catalyst consists only of well-crystallized α-$NiMoO_4$ particles. Supporting this phase on the activated carbons, results in poor and highly disordered crystallization, while a change in the phases formed also occurs. All three bimetallic AC supported catalysts share similar structural characteristics and are in general more amorphous with smaller crystallites than the monometallic ones. Ni and MoO_2 crystallites are detected along with small amounts of α- and mainly β-$NiMoO_4$ mixed phases, where Mo is in octahedral and tetrahedral coordination respectively [27,28]. Previous studies [29,30] have suggested that β-$NiMoO_4$, which is only stable at high temperatures, shows better catalytic behavior than the α-phase. Recent studies [31,32] have shown that this phase can be stabilized, even at room temperature, in supported $NiMoO_4$ catalysts, while the relative amount of the α- and β-phase depends on the content of $NiMoO_4$ [33]. Therefore, the transition observed from the α- to the β-$NiMoO_4$ phase in the AC supported catalysts could be attributed to the stabilization of the latter on the surface of the support. Comparing the two different supports, slightly lower peak intensity can be observed for the AC2 supported catalysts with the larger surface area, indicating better active phase dispersion on this support.

The reducibility of the materials was studied by temperature programmed reduction with hydrogen. Fig. 3 illustrates the H_2 consumption profiles of all the AC-supported catalysts. The reduction profiles of the calcined acid treated AC1 support and the unsupported K—NiMo phase are also presented for comparison reasons. The quantitative results of the TPR in terms of hydrogen consumption are shown in Table 2. The unsupported K—NiMo catalyst, consisting of well-crystallized α-$NiMoO_4$ phase as indicated by the XRD results, exhibits large hydrogen consumption from 500 to 700 °C, with two main peaks at 550 °C and ~650 °C, in agreement with most results previously reported by other authors [33–35]. Differences in the maximum temperature of reduction in comparison to literature can occur due to different experimental reduction conditions (e.g. heating rates). According to Rodriguez et al. [28] and Brito et al. [34], the mixed α-$NiMoO_4$ phase is most likely to reduce toward Ni_4Mo, Ni and NiO. However, the mechanism of H_2-reduction of α-$NiMoO_4$ is still debated, especially at temperatures below 500 °C.

The pure calcined AC1a support demonstrates very low reducibility, with a wide reduction peak extending from 400 to 750 °C and a maximum at ~600 °C (Fig. 3), attributed to the reduction of oxygen-containing functional groups. Similar results were obtained for all activated carbon supports (not shown), with hydrogen consumption ranging from 0.6 to 2 mmol/g. Concerning the monometallic catalysts, the K—Ni/AC1a catalyst does not reduce significantly, as expected, since metallic Ni is the only phase formed upon heating the impregnated catalysts at 575 °C in N_2 atmosphere. The low reduction observed could be attributed to the reduction of the support, shifted to ~100 °C lower temperature due to the presence of nickel. Similar results are obtained also for the monometallic K—Mo/AC1a, with a wide peak centered at 500 °C due to the support reduction. However, an additional small peak is observed at ~700 °C that could be attributed to partial reduction of Mo(IV) to lower oxidation states, as Mo in this catalyst exists primarily as MoO_2 (Fig. 2). According to Kim et al. [36], MoO_2 is reduced at temperatures above 630 °C, due to its cluster characteristics, i.e. Mo—Mo bond-like interactions, that render it resistant to reduction [34]. All bimetallic K—NiMo catalysts supported on the various AC supports share similar reduction profiles. The main reduction peak is located at 440 °C and can be attributed to the reduction of the β-$NiMoO_4$ phase which was identified in these materials by XRD. This agrees with the work of Dias et al. [33] and Del Rosso et al. [37] suggesting that β-$NiMoO_4$ is easier reduced than α-$NiMoO_4$. All samples also demonstrate a smaller peak at 610 °C, which can be assigned to partial reduction of tetravalent molybdenum.

During H_2 TPR, desorption of CO, together with minor amounts of CO_2, at 600–800 °C was detected in all samples (Fig. 3). Desorption of carbon oxides can be attributed to the decomposition of various types of surface oxygen groups (i.e. phenol, carbonyl, quinone, ether and pyrene groups), weakly acidic, neutral and basic groups where C is bonded to an oxygen atom [24]. However, the quantity of desorbed CO (see Table 2) is much higher from the monometallic Mo and all bimetallic NiMo catalysts compared to the pure activated carbon supports, with a desorption temperature of 750 °C and 650 °C respectively (Fig. 3). On the contrary, significantly less CO desorbs from the K—Ni/AC1a catalyst, while no CO or CO_2 formation was recorded over the reference unsupported K—NiMo phase. All the above indicate that CO is formed and desorbed only from the AC supported catalytic samples which contain the active phase in an oxidic form. It can be postulated that as the oxidic phases are reduced in the presence of hydrogen, some oxygen and/or water reacts with the carbon support and partially oxidizes a small fraction to carbon monoxide.

The ammonia desorption curves of all the AC-supported catalysts and the unsupported K—NiMo reference phase are compiled in Fig. 4. The acidity of all catalysts (expressed as mol of desorbed NH_3/m^2) is given in Table 2. The K—Ni/AC1a catalyst shows negligible acidity (in the same range as the activated carbon support), demonstrating that metallic Ni does not provide any acidity. A moderate increase in acidity is attained for the K—Mo/AC1a catalyst, as weak acid sites with a maximum desorption temperature at 200 °C are detected, probably attributed to MoO_2. The bimetallic K—NiMo/AC1a catalyst exhibits a much higher acidity, demonstrated by desorption of large amounts of ammonia at 250 °C attributed to weak/medium acid sites. Small ammonia desorption

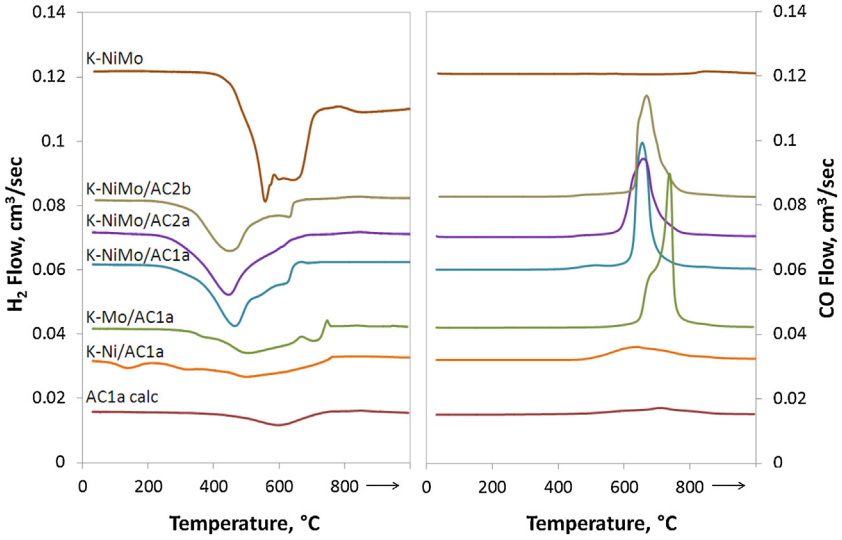

Fig. 3. Temperature-programmed reduction profiles of the K-promoted mono- and bi-metallic NiMo catalysts and reference unsupported K—NiMo and AC1a$_{calc}$ support.

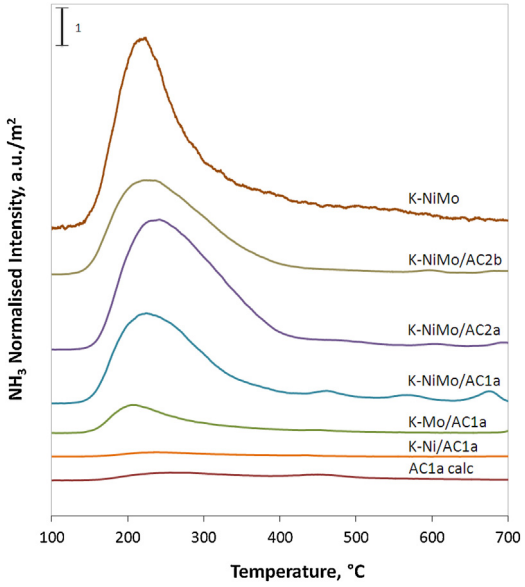

Fig. 4. Ammonia desorption profiles of the K-promoted mono- and bi-metallic NiMo catalysts and reference unsupported K—NiMo and AC1a$_{calc}$ support.

peaks can also be observed at very high temperature (>600 °C), indicating that the catalyst accommodates on the surface some strong acid sites as well. The acidity of the bimetallic catalyst is much higher than the sum of the two monometallic ones, indicating a strong synergistic effect between Ni and Mo and the formation of Ni—O—Mo bonds with acidic function. This acidic functionality could be related to electron donation from Ni to Mo. In general, all K-promoted bimetallic catalytic materials exhibit a well-defined desorption peak extending from 150 to 400 °C, with a maximum at ~220 °C, assigned to weak/medium acid sites. Comparing the two different surface area carbon supports, it can be observed that the acidity of the K—NiMo/AC2a catalyst is about 20% higher compared to that of K—NiMo/AC1a. It can be therefore conjectured that the higher surface of the AC support induces a higher dispersion of the acidic mixed NiMo phase, resulting in higher number of exposed acidic active sites. Comparing the acidity of the catalysts based on acid treated and untreated AC2 support (see Table 2), the K—NiMo/AC2a catalyst demonstrates higher acidity due to the formation of oxygen surface groups via the treatment with HNO_3 [21]. This is in agreement with the acidity measurements of the pure supports, which showed that the acid treated AC2a is more acidic than the corresponding untreated sample even after calcination at 575 °C, indicating that acid treatment leads to creation of stable acidic functionalities on the surface of the activated carbons. The unsupported K—NiMo catalyst appears to have the highest amount of acid sites per m^2, but this is due to its relatively very low surface area compared to the supported catalysts. The acidity of the unsupported phase on a weight basis is as expected much lower (an order of magnitude) than that of the supported catalysts due to the lower exposure of surface acidic sites.

3.2. Catalytic performance in CO hydrogenation to higher alcohols

3.2.1. Effect of active metal component

The performance of the K-promoted monometallic Ni/AC1a, Mo/AC1a and the bimetallic NiMo/AC1a catalysts in the higher alcohol synthesis reaction at 250 °C and 280 °C is shown in Table 3. Overall, both K-promoted Ni and Mo monometallic catalysts appear to be extremely less active in CO hydrogenation under the current experimental conditions, compared to the respective bimetallic one, as was similarly reported by Zhao et al. [38]. More specifically, the maximum CO conversion attained at 280 °C is 0.3% and 1.5% for the K—Ni/AC1a and the K—Mo/AC1a respectively, compared to 13.5% for the K—NiMo/AC1a. This shows that the Ni—Mo synergistic effect is mandatory in order to achieve a satisfactory activity under the investigated conditions. In agreement with our results, Li et al. [8] who studied CO hydrogenation reaction over monometallic K–Mo/AC catalysts, reported similar CO conversions at the same temperature range. The main reaction products over the catalysts were C_1–C_6 alcohols, dimethyl ether (DME), C_1–C_8 hydrocarbons, as well as CO_2 resulting from the WGS side-reaction. The product distribution on a CO_2-free basis, as well as the yield to total oxygenates (methanol, higher alcohols and DME), is shown in Table 3. Selectivities are not provided for the monometallic catalysts, as the CO conversion for K—Ni/AC1a and K—Mo/AC1a was very low and therefore the collected liquid sample from cold trap was very limited. This could entail major errors in the calculation of the selectivity to the different products, thus providing misleading results. The K-promoted bimetallic NiMo/AC1a catalyst demonstrates an acceptable selectivity to alcohols at 250 °C, which decreases with increasing temperature, accompanied by an

Table 3
Catalytic performance of the K-promoted mono- and bi-metallic NiMo catalysts.

Samples	Temperature (°C)	CO conversion (%)	Total oxygenates STY ($mg/g_{cat}/h$)	Carbon selectivity (CO_2 free) (C mol%)			
				MeOH	$C_{2+}OH$	DME	HC
K—Ni/AC1a	250	0.2	2.8	N/A	N/A	N/A	N/A
	280	0.3	5.0	N/A	N/A	N/A	N/A
K—Mo/AC1a	250	0.6	6.2	N/A	N/A	N/A	N/A
	280	1.5	9.2	N/A	N/A	N/A	N/A
K—NiMo/AC1a	250	5.3	26.9	9.1	18.4	28.7	43.8
	280	13.5	68.1	4.9	6.4	35.3	53.4
K—NiMo/AC2a	250	7.9	62.0	15.9	17.8	26.5	39.8
	280	25.0	141.5	8.3	7.8	29.6	54.3
K—NiMo/AC2b	250	4.7	37.0	18.6	15.0	24.9	41.5
	280	12.1	80.6	11.7	12.0	28.4	47.9
K—NiMo	250	14.7	90.9	5.6	5.6	33.6	55.2
	280	35.8	193.9	3.9	2.1	35.8	58.2

Reaction conditions: $P = 60$ bar, $W/F = 0.63$ g s/cm^3, $H_2/CO = 2$.

increase in the selectivity to DME and hydrocarbons. In terms of performance toward all oxygenated products, the above catalyst exhibits a high space time yield of 68 $mg/g_{cat}/h$ at 280 °C. In contrast, the maximum oxygenates space time yield (STY) achieved with K–Ni/AC1a and K–Mo/AC1a is 13.5 and 7 times less than the K-promoted bimetallic NiMo/AC1a, respectively, due to the low reactivity of the K-promoted monometallic Ni and Mo catalysts.

Since both Mo and Ni alone seem inactive for hydrogenating CO under the present reaction conditions, activation of CO and formation of oxygenates could be clearly attributed to the Ni—Mo synergetic interaction. Combining the activity results with the acidity measurements, it becomes clear that the synergy between Ni and Mo leads to great increase in both acidity and activity toward CO, pointing out to Ni—O—Mo acid sites being the active phase for carbon monoxide adsorption and activation. The mixed Ni_6Mo_6C, "Co_3Mo_3C" and "Ni—Mo—S" phases have been suggested to be responsible for the high activity of higher alcohol synthesis in similar catalysts [39–41]. Nagai et al. [42] reported that carbon-deficient Ni_6Mo_6C crystallites constitute the active sites in Ni—Mo bimetallic carbide catalysts. They suggested that CO adsorbs molecularly rather than dissociatively on the Ni- and C-terminated surface defect sites of the Ni—Mo bimetallic carbide catalysts, leading to oxygenate rather than hydrocarbon formation. Similar results for CO adsorption on CoMo carbides were also reported by Nagai and Matsuda [43].

3.2.2. *Effect of type and pre-treatment of activated carbon support*

In addition to the low surface area AC1 (600 m^2/g), a high surface area activated carbon (AC2 with 1150 m^2/g) was also used as support of the metal active phases. As can be seen from the data in Table 3 the K—NiMo/AC2a catalyst exhibits the maximum CO conversion activity (25% at 280 °C) amongst all the AC supported catalysts, while the unsupported K—NiMo catalyst shows even higher activity, with a CO conversion of 35.8% at 280 °C. However, if one considers that in the supported bimetallic catalysts, the weight percentage of the metals is approximately 35% (close to 50% if we consider the oxide form), then it becomes clear that these supported phases are more reactive, at least on a catalyst mass basis comparison, compared to the unsupported one.

Comparing the two carbon supports AC1a and AC2a (after acid treatment), the K—NiMo/AC2a catalysts clearly demonstrates higher reactivity than K—NiMo/AC1a. Although the final surface area of the two catalysts was not very different (425 m^2/g and 325 m^2/g respectively), the initial AC2 support has a surface area twice as big as that of AC1. The much higher activity of the catalyst supported on AC2, especially at 280 °C, can be attributed to better dispersion of the active phase on the higher surface area support and therefore higher exposure of active sites on the surface, as indicated by the less crystalline nature of the metal phases (XRD patterns) and the acidity results. In terms of product selectivity, alteration of the AC support induces only small changes, with the K—NiMo/AC2a catalyst exhibiting higher methanol and lower DME and HC selectivity compared to AC1a. Fig. 5 illustrates a detailed distribution of the products over the K—NiMo/AC2a sample at 250 and 280 °C. Similar behavior was observed for all K-promoted bimetallic Ni—Mo catalysts. Generally it can be observed that the synthesis yields preferentially DME, low molecular weight hydrocarbons and linear alcohols with up to four carbon atoms. According to a review by Surisetty et al. [6] the alcohol products over alkali-promoted molybdenum-based catalysts are linear alcohols and the mechanism for formation of higher alcohols is via a classical insertion of CO into the corresponding precursor alcohol [44]. The presence however of secondary alcohols in the product mix suggests that chain-growth also takes place via an aldol condensation pathway. Evidence of the occurrence of alcohol coupling reactions over sulfided Mo-based catalysts has also been reported by Christensen et al. [45].

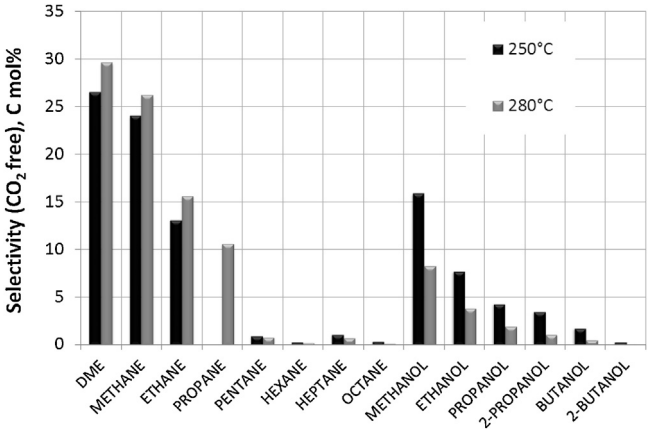

Fig. 5. Products selectivity (CO_2-free) over the K—NiMo/AC2a catalyst at 300 and 320 °C (reaction conditions: $P = 60$ bar, $W/F = 0.63$ g s/cm^3, $H_2/CO = 2$).

The carbon-based CO_2 free selectivity presented in Table 3 shows that on all bimetallic samples the increase of temperature (and conversion) brings about a sharp increase in hydrocarbons and DME concentration, at the expense of alcohols formation. Higher temperatures enhance significantly the formation of hydrocarbons

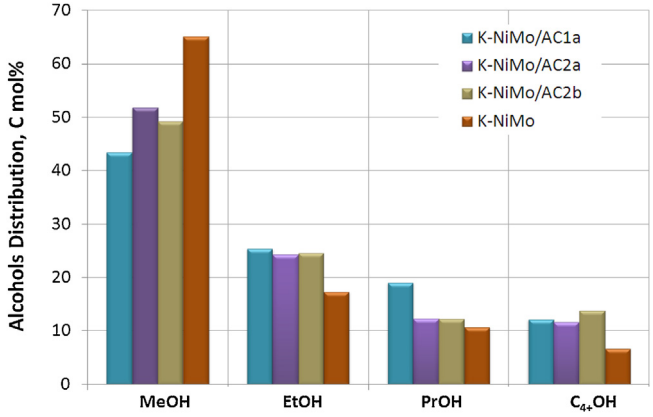

Fig. 6. Alcohols distribution over the K-promoted bimetallic NiMo catalysts supported on different activated carbon supports (reaction conditions: $T = 280\,^{\circ}C$, $P = 60$ bar, $W/F = 0.63$ g s/cm^3, $H_2/CO = 2$).

and CO_2, in agreement with our previous results regarding higher alcohols formation over Cu-based catalysts [46]. Xiaoding et al. [47] and Tien-Thao et al. [48] have also reported that CO_2 formation is favored at higher temperatures, resulting in a change in the H_2/CO ratio, which directly affects the higher alcohol formation. Another possible explanation would be related to higher activation energy for hydrogenation than for CO insertion in the carbonaceous intermediate [8].

The effect of pre-treating the support with acid can be evidenced by comparing the catalytic performance of the K—NiMo/AC2a and K—NiMo/AC2b samples. In terms of reactivity, it is clear that acid treatment favors CO conversion, with the catalyst supported on acid treated carbon exhibiting double CO activation. This can be attributed to the higher acidity of K—NiMo/AC2a, possibly providing a higher population of active acidic sites on the mixed oxides for CO activation. The higher acidity and activity could in turn be related with the much lower ash content in the acid treated support, as determined by TGA and ICP (Figure S2 and Table S2 in Supplementary material). The removal of the ash "cleans" the surface and thus allows the formation of more surface carbon–oxygen complexes that can enhance metal dispersion on the support. Regarding product formation, the main change that occurs from the acid pre-treatment of the support is the reduced selectivity toward methanol at both reaction temperatures and toward higher alcohols at 280 °C (see Table 3). Previously reported results by several researchers indicate that support basicity facilitates the alcohols production providing basic sites for the aldol-type condensation of lower to higher alcohols [3,49]. It has to be noted here that both the parent activated carbons used (AC1 and AC2) provided an alkaline pH when dispersed in water. It can be thus assumed that less acidity is required on the catalysts for the various C—C and C—O bond-forming reactions to take place.

For the unsupported K—NiMo, higher selectivity to hydrocarbons and DME and lower selectivity to alcohols was obtained compared to the supported catalysts. According to the XRD results, the observed crystalline phase on the unsupported catalyst is only the alpha form of the $NiMoO_4$ phase and not the beta form, which might constitute the active site for alcohol synthesis. Among alcohols, the absence of the support favors the formation of methanol and reduces the homologation of the alcohol chain. The detailed distribution of the alcohols, illustrated in Fig. 6, shows that over the unsupported K—NiMo catalyst the highest concentration of methanol is attained, followed by descending amounts of ethanol, propanol and C_{4+}OH. Thus, the unsupported catalyst is not suitable for higher alcohol synthesis, as it exhibits the lowest selectivity to higher products among the studied catalysts. Similar conclusions

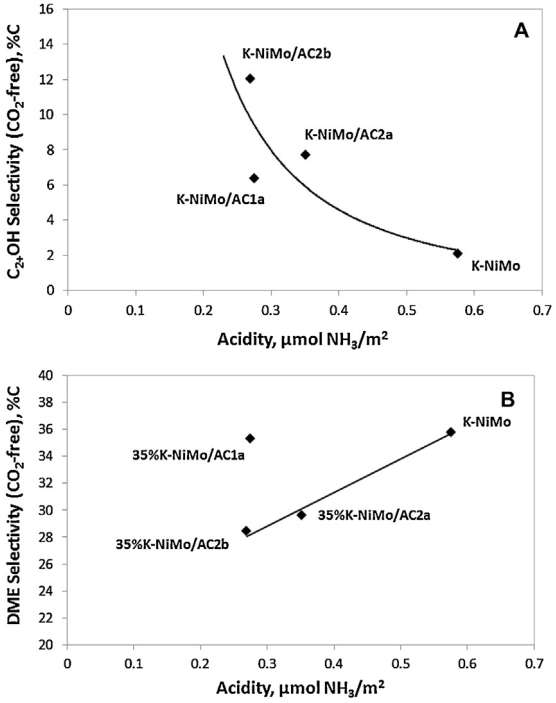

Fig. 7. Total acidity as a function of (a) higher alcohols selectivity and (b) DME selectivity at 280 °C for all K-promoted bi-metallic NiMo catalysts (reaction conditions: $T = 280\,^{\circ}C$, $P = 60$ bar, $W/F = 0.63$ g s/cm^3, $H_2/CO = 2$).

were also drawn by Ma et al. [18] who compared product yields and selectivities over K—NiMo unsupported and supported catalysts. Their results also clearly showed that the unsupported bimetallic catalyst results in a poorer higher alcohol synthesis catalyst. Comparing the alcohols distribution over the AC supported catalysts, the most appreciable changes compared to the reference are recorded for the K—NiMo/AC1a catalyst. A significant decrease in methanol formation is evidenced, with concurrent increase in propanol formation (Fig. 6). Regarding the effect of the AC acid treatment, no significant variation is observed on alcohols distribution.

Overall, the K—NiMo/AC2a catalyst exhibits the optimum performance, with high CO conversion at 280 °C and high production of oxygenates. The catalyst demonstrates a space time yield of 141.5 mg/$g_{catalyst}$/h to oxygenates at 280 °C, which is the highest amongst all the AC supported samples. Although the unsupported K—NiMo exhibits the highest CO conversion and oxygenates production (see Table 3), the C_{2+} alcohols to total oxygenates STY ratio is 0.04, whereas the corresponding ratio for the K—NiMo/AC2a is 0.15. These results render the K—NiMo/AC2a catalyst as the most active among the investigated materials for CO hydrogenation to higher alcohols.

3.3. Correlation between acidity and higher alcohols formation

In a previous work by our group on K-promoted Cu—Zn—Al catalysts for higher alcohol synthesis [46], an inverse correlation between acidity and higher alcohols selectivity was established, indicating that reduced acidity favors aldol-type condensation reactions and thus production of higher alcohols. Previously reported results by several researchers indicate that the basicity of the support facilitates the production of alcohols and other oxygenated compounds for Mo-based catalysts, in a similar way [50–52]. Other reports suggest that acidic sites on supports favor DME and hydrocarbon formation, thus causing a reduction in alcohol selectivity [53]. In light of this, selectivity to higher alcohols at 280 °C is plotted as a function of total acidity in Fig. 7a for all the

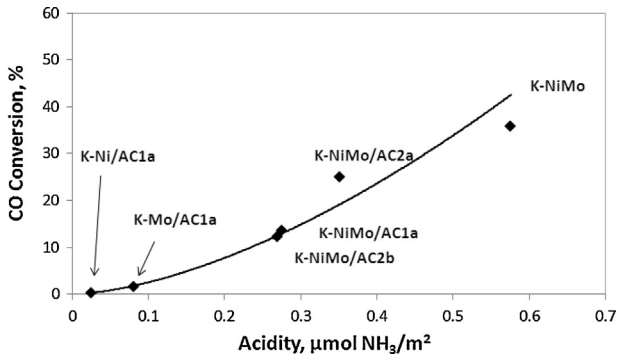

Fig. 8. Total acidity as a function of CO conversion at 280 °C for all K-promoted mono- and bi-metallic NiMo catalysts (reaction conditions: T = 280 °C, P = 60 bar, W/F = 0.63 g s/cm^3, H_2/CO = 2).

investigated K-promoted bimetallic catalysts. Although selectivity values were not attained at identical conversion levels, conversion is within reasonable comparison range. The K-promoted monometallic catalysts are not included in this comparison, since CO conversion was extremely low and in addition, collected liquid product in these experiments was very limited thus selectivity values are uncertain. A clear tendency of increasing higher alcohol selectivity with decreasing acidity is apparent, in accordance with the general notion that higher alcohol formation requires basic sites. The use of the non-treated support reduces acidity and thus promotes the production of the desired higher alcohol products. Fig. 7b illustrates DME selectivity at 280 °C as a function of total acidity. Increasing DME production with ascending acidity is observed as expected, since acid sites are responsible for methanol dehydration to DME reaction [54–56]. As a result an increased DME selectivity at the expense of alcohols production is observed. It can also be observed that the K—NiMo/AC1a catalyst deviates from linearity, demonstrating higher DME selectivity than would be expected based on its acidity. This could be attributed to the fact that selectivity to DME depends not only on number of acid sites, but also on the strength of acid sites [57]. The K—NiMo/AC1a sample was the only material that demonstrated strong acid sites; therefore this deviation can be attributed to the presence of this strong acidity on the catalyst.

Having said that, it was also clearly shown in the catalytic experiments that although acidity negatively affects the formation of higher alcohols, it is clearly related with increased CO activity. Fig. 8 presents the CO conversion attained at 280 °C as a function of catalyst acidity. CO conversion seems to exponentially increase with acidity for all samples. As discussed in previous paragraphs, both acidity and conversion of the monometallic Ni and Mo catalysts is negligible. The interaction between Ni and Mo leads to formation of mixed Ni—O—Mo bonds which exhibit acidic functionalities (probably due to electron donation from Ni to Mo) and to increased affinity to CO, pointing out to these mixed phases being the active sites for CO activation. Concerning the bimetallic NiMo catalysts, the differences in acidity (and activity) are probably a result of better dispersion of the active phase on the catalytic surface area, depending on the initial surface area of the AC support. Similar trends of increasing CO conversion with acidity have been reported over Cu-based catalysts. Wu et al. [20] reported correlation between acid site concentration and conversion for Cu—Ni catalysts supported on different supports with varying acidity. Also Jeong et al. [58] proved a direct correlation between the catalyst acid sites and CO conversion, in agreement with Das et al. [59] who claim that CO absorbs on weak acid sites in order to carry out the Fischer–Tropsch reaction, thus increased activity with acidity is observed. However, to the best of our knowledge, such correlations have not been identified for CO activation on Mo-based catalysts. Our study indicates that although acidity reduces selectivity to the desired products, acid sites seem to be necessary for CO activation. Optimum higher alcohol synthesis catalysts should therefore have a balanced amount of acid sites, with a trade-off between high conversion and high HAS formation.

4. Conclusions

The aim of the current study was to investigate the effect of active metal and the nature and pre-treatment of the support in a series of K-promoted NiMo catalysts supported on activated carbon for the hydrogenation reaction of CO. Monometallic Ni and Mo AC-supported catalysts both proved to be inactive in CO hydrogenation under the investigated conditions, demonstrating that the Ni—Mo synergistic effect and the formation of Ni—O—Mo functionalities is mandatory in order to produce a fair amount of oxygenates.

The effect of supporting the active phase on activated carbon and the influence of the type of the carbon used as support were examined by employing two activated carbons with significantly different textural properties. Although the unsupported K—NiMo phase exhibited a higher activity, it mainly produced hydrocarbons and DME rather than alcohols. The use of activated carbon as support led to a minimum three-fold increase in the selectivity toward higher alcohols. Characterization revealed that the presence of the support reduces the crystallinity of the $NiMoO_4$ phase in the samples and leads to a partial transformation of this mixed oxide from the alpha to the beta-phase. Subjecting the activated carbon to acidic pre-treatment prior to active metal deposition led to double CO conversion for the K—NiMo/AC2a catalyst compared to the untreated one (K—NiMo/AC2b). This could be related the removal of ash from the activated carbon support and the improved dispersion of the active phase, as indicated by the increased acidity of the catalyst. In terms of products, acid pre-treatment led to reduced methanol and higher alcohol selectivity as a result of the high acidity. Finally, the use of a higher surface area support led to increased CO reactivity, with the K—NiMo/AC2a exhibiting a 45% higher conversion at 280 °C compared to K—NiMo/AC1a. The improvement in activity can be ascribed to better dispersion of the active phase on the higher surface area support and therefore higher exposure of active sites on the surface, as indicated by the less crystalline nature of the particles and the acidity results. Overall, the K—NiMo/AC2a catalyst exhibited the optimum performance, with high CO conversion (25% at 280 °C) and high production of oxygenates, with a space time yield to oxygenates of 141.5 mg/$g_{catalyst}$/h at 280 °C. It should be mentioned however that on a carbon efficiency basis, the catalytic performance is not optimum and further improvement of the catalytic system is needed for industrial implementation.

In general, a clear tendency of increasing higher alcohol with decreasing acidity was evidenced. However, an undisputed correlation between CO conversion and acidity was established for all catalysts, indicating that Ni—O—Mo entities with acidic properties constitute the actives centers for CO activation.

Acknowledgments

These results have been achieved within the framework of the project “European Multilevel Integrated Biorefinery Design for Sustainable Biomass Processing – EuroBioRef”, funded by the EU under the 7th Framework Programme of the European Union for the funding of research and technological development in Europe. The author Eleni Liakakou would like in addition to acknowledge financial support from European Union (European Social Fund – ESF) and Greek national funds through the Operational Program “Education and Lifelong Learning” of the National Strategic Reference

Framework (NSRF) – Research Funding Program: THALES. Investing in knowledge society through the European Social Fund.

Appendix A. Supplementary data

Supplementary material related to this article can be found, in the online version, at http://dx.doi.org/10.1016/j.apcatb.2014.10.027.

References

[1] Eurobioref Public Booklet, Available from: http://eurobioref.org/images/Eurobioref_livret_resultats_total_v4.pdf [April 2014].
[2] R.G. Herman, Catal. Today 55 (2000) 233–245.
[3] J.J. Spivey, A. Egbebi, Chem. Soc. Rev. 36 (2007) 1514–1528.
[4] V. Subramani, S.K. Gangwal, Energy Fuels 22 (2008) 814–839.
[5] S. Zaman, K.J. Smith, Cat. Rev. – Sci. Eng. 54 (1) (2012) 41–132.
[6] V.R. Surisetty, A.K. Dalai, J. Kozinski, Appl. Catal. A: Gen. 404 (2011) 1–11.
[7] T. Tatsumi, A. Muramatsu, H.O. Tominaga, Chem. Lett. (1984) 685–688.
[8] X. Li, L. Feng, L. Zhang, D.B. Dadyburjor, E.L. Kugler, Molecules 8 (2003) 13–30.
[9] V.R. Surisetty, A. Tavasoli, A.K. Dalai, Appl. Catal., A 365 (2009) 243–251.
[10] S. Zaman, K.J. Smith, Appl. Catal., A 378 (2010) 59–68.
[11] A. Muramatsu, T. Tatsumi, H. Tominaga, Bull. Chem. Soc. Jpn. 60 (1987) 3157–3161.
[12] H.J. Qi, D.B. Li, C. Yang, Y.G. Ma, W.H. Li, Y.H. Sun, B. Zhong, Catal. Commun. 4 (2003) 339–342.
[13] E.C. Alyea, D. He, J. Wang, Appl. Catal., A 104 (1993) 77–85.
[14] J.G. Santiesteban, C.E. Bogdan, R.G. Herman, K. Klier, 9th Int. Congr. Catal., Chemical Institute of Canada, Ottawa, 1988.
[15] J. Iranmahboob, D.O. Hill, H. Toghiani, Appl. Catal. A: Gen. 231 (2003) 99–108.
[16] B.E. Concha, G.L. Bartholomew, C.H. Bartholomew, J. Catal. 89 (1984) 536–541.
[17] V.R. Surisetty, I. Eswaramoorthi, A.K. Dalai, Fuel 96 (2012) 77–84.
[18] C.-H. Ma, H.-Y. Li, G.-D. Lin, Catal. Lett. 137 (2010) 171–179.
[19] J.-J. Wang, J.-R. Xie, Y.-H. Huang, B.-H. Chen, G.-D. Lin, H.-B. Zhang, Appl. Catal. A: Gen. 468 (2013) 44–51.
[20] Q. Wu, A.D. Jensen, J.-D. Grunwaldt, B. Temel, J.M. Christensen, Catalytic synthesis of alcoholic fuels for transportation from syngas (PhD thesis), Technical University of Denmark, Department of Chemical Engineering, 2013.
[21] S. Wang, J.Q. Lu (Max), Carbon 36 (3) (1998) 283–292.
[22] F. Rouquerol, J. Rouquerol, K. Sing, Adsorption by Powders & Porous Solids, Academic Press, San Diego, 1999.
[23] N. Passe-Coutrin, S. Altenor, D. Cossement, C. Jean-Marius, S. Gaspard, Microporous Mesoporous Mater. 111 (2008) 517–522.
[24] G. De la Puente, A. Centeno, A. Gil, P.J. Grange, Colloid Interface Sci. 202 (1998) 155–166.
[25] L.M. Gandia, M. Montes, J. Catal. 145 (1994) 276–288.
[26] J. Li, Y. Fu, M. Jiang, T. Hu, T. Liu, Y. Xie, J. Catal. 199 (2001) 155–161.
[27] H.M. AbdelDayem, M.A. Al-Omair, Ind. Eng. Chem. Res. 47 (2008) 1011–1016.
[28] J.A. Rodriguez, J.Y. Kim, J.C. Hanson, J.L. Brito, Catal. Lett. 82 (1–2) (2002) 103–109.
[29] C. Mazzocchia, C. Aboumrad, C. Diagne, E. Tempesti, J.M. Herrmann, G. Thomas, Catal. Lett. 10 (3–4) (1991) 181–191.
[30] J.L. Brito, A.L. Barbosa, A. Albornoz, F. Severino, J. Laine, Catal. Lett. 26 (1994) 329–337.
[31] D. Cauzzi, M. Deltratti, G. Predieri, A. Tripicchio, A. Kaddouri, C. Mazzocchia, E. Tempesti, A. Armigliato, C. Vignali, Appl. Catal. A: Gen. 182 (1999) 125–135.
[32] R. Zavoianu, C.R. Dias, M.F. Portela, Catal. Commun. 2 (2001) 37–42.
[33] C.R. Dias, R. Zavoianu, M.F. Portela, Catal. Commun. 3 (2002) 85–90.
[34] J.L. Brito, J. Laine, K.C.J. Pratt, Mater. Sci. 24 (1989) 425–431.
[35] L.M. Madeira, M.F. Portela, C. Mazzocchia, A. Kaddouri, R. Anouchinsky, Catal. Today 40 (1998) 229–243.
[36] B.-S. Kim, E. Kim, H.-S. Jeon, H.-I. Lee, J.-C. Lee, Mater. Trans. 49 (2008) 2147–2152.
[37] R. Del Rosso, A. Kaddouri, C. Mazzocchia, P. Gronchi, P. Centola, Catal. Lett. 69 (2000) 71–78.
[38] L. Zhao, K. Fanga, D. Jianga, D. Li, Y. Sun, Catal. Today 158 (2010) 490–495.
[39] M.L. Xiang, D.B. Li, W.H. Li, B. Zhong, Y.H. Sun, Catal. Commun. 8 (2007) 503–507.
[40] D.B. Li, C. Yang, H.R. Zhang, W.H. Li, Y.H. Sun, B. Zhong, Stud. Surf. Sci. Catal. 147 (2004) 391–396.
[41] D.B. Li, C. Yang, H.J. Qi, W.H. Li, Y.H. Sun, B. Zhong, Catal. Commun. 5 (2003) 605–609.
[42] M. Nagai, A.Md. Zahidul, K. Matsuda, Appl. Catal. A: Gen. 313 (2006) 137–145.
[43] M. Nagai, K. Matsuda, J. Catal. 238 (2006) 489–496.
[44] H.C. Woo, K.Y. Park, Y.G. Kim, I.-S. Namau, J.S. Chung, J.S. Lee, Appl. Catal. 75 (1991) 267–280.
[45] J.M. Christensen, P.A. Jensen, N.C. Schiødt, A.D. Jensen, ChemCatChem 2 (2010) 523–526.
[46] E. Heracleous, E.T. Liakakou, A.A. Lappas, A.A. Lemonidou, Appl. Catal., A 455 (2013) 145–154.
[47] X. Xiaoding, E.B.M. Doesburg, J.J.F. Scholten, Catal. Today 2 (1987) 125–170.
[48] N. Tien-Thao, H.M. Zahedi-Niaki, H. Alamdari, S. Kaliaguine, J. Catal. 245 (2007) 348–357.
[49] J.T. Kozlowski, R.J. Davis, ACS Catal. 3 (2013) 1588–1600.
[50] X. Li, L. Feng, Z. Liu, B. Zhong, D.B. Dadyburjor, E.L. Kugler, Ind. Eng. Chem. Res. 37 (1998) 3858–3863.
[51] H. Okatsu, M.R. Morrill, H. Shou, D.G. Barton, D. Ferrari, R.J. Davis, P.K. Agrawal, C.W. Jones, Catal. Lett. 144 (2014) 825–830.
[52] H. Shou, R.J. Davis, J. Catal. 282 (2011) 83–93.
[53] G.-Z. Bian, L. Fan, Y.-L. Fu, K. Fujimoto, Ind. Eng. Chem. Res. 37 (1998) 1736–1743.
[54] M. Xu, J.H. Lunsford, D.W. Goodman, A. Bhattacharyya, Appl. Catal., A 149 (1997) 289–301.
[55] I. Sierra, J. Ereña, A.T. Aguayo, J.M. Arandes, J. Bilbao, Appl. Catal. B: 94 (2010) 108–116.
[56] F.S. Ramos, A.M. Duarte de Farias, L.E.P. Borges, J.L. Monteiro, M.A. Fraga, E.F. Sousa-Aguiar, L.G. Appel, Catal. Today 101 (2005) 39–44.
[57] E.F. Sousa-Aguiar, L.G. Appel, in: J.J. Spivey, K.M. Dooley (Eds.), Catalysis, vol. 23, RSC, 2011, pp. 284–315.
[58] J.W. Jeong, C.-I. Ahn, D.H. Lee, S.H. Um, J.W. Bae, Catal. Lett. 143 (2013) 666–672.
[59] S.K. Das, S. Majhi, P. Mohanty, K.K. Pant, Fuel Process. Technol. 118 (2014) 82–89.